Corneal regenerative contribution of endogenous and grafted limbal-corneal cells in a mouse model of simple limbal-corneal epithelial transplantation

Marcia F D Costa, PhD, Nicola Piazza, MSc, Erika Bonacci, MD, Sissi Dolci, PhD, Francesca Ciarpella, PhD, Marzia Di Chio, HSD, Stefania Zorzin, PhD, Andrea Corsi, PhD, Alessandro Piva, PhD, Cristiano Chiamulera, PhD, Zulkifal Malik, PhD, Riccardo Esposito, MSc, Francesco Bifari, MD, PhD, Stefano Ugel, PhD, Adriano Fasolo, MSc, Antonella Motta, PhD, Stefano Ferrari, PhD, Emilio Pedrotti, MD, Ilaria Decimo, PhD

Stem Cells Translational Medicine, 2026, **15**, szag007
https://doi.org/10.1093/stcltm/szag007
Original Research

Corneal regenerative contribution of endogenous and grafted limbal-corneal cells in a mouse model of simple limbal-corneal epithelial transplantation

Marcia F.D. Costa, PhD[1], Nicola Piazza, MSc[1], Erika Bonacci, MD[2], Sissi Dolci, PhD[1], Francesca Ciarpella, PhD[1], Marzia Di Chio, HSD[1], Stefania Zorzin, PhD[1], Andrea Corsi, PhD[1], Alessandro Piva, PhD[3], Cristiano Chiamulera, PhD[3], Zulkifal Malik, PhD[4], Riccardo Esposito, MSc[4], Francesco Bifari, MD, PhD[4], Stefano Ugel, PhD[5], Adriano Fasolo, MSc[6,7], Antonella Motta, PhD[8,9], Stefano Ferrari, PhD[6], Emilio Pedrotti, MD[7,*], Ilaria Decimo, PhD[*,1]

[1]Laboratory of Pharmacology, Department of Diagnostics and Public Health, University of Verona, Verona 37134, Italy
[2]Department of Engineering for Innovation Medicine, Ophthalmology Clinic, University of Verona, Verona 37134, Italy
[3]Laboratory of Neuropsychopharmacology, Section Pharmacology, Department Diagnostic and Public Health, University of Verona, Verona 37134, Italy
[4]Laboratory of Cell Metabolism and Regenerative Medicine, Department of Medical Biotechnology and Translational Medicine, University of Milan, Milan 20054, Italy
[5]Section of Immunology, Department of Medicine, University of Verona, Verona 37134, Italy
[6]Veneto Eye Bank Foundation, Venice 30174, Italy
[7]Department of Surgery, Dentistry, Pediatrics and Gynecology, Ophthalmology Clinic, University of Verona, Verona 37134, Italy
[8]Department of Industrial Engineering and BIOTech Research Center, University of Trento, Trento 38123, Italy
[9]Department of Pharmaceutical Sciences, Chulalongkorn University, Bangkok 10330, Thailand

*Corresponding authors. Ilaria Decimo, Laboratory of Pharmacology, Department of Diagnostic and Public Health, University of Verona, P.le L.A. Scuro n. 10, Verona, 37134, Italy. E-mail: ilaria.decimo@univr.it; Emilio Pedrotti, Department of Surgical Sciences, Dentistry and Maternal-Child, University of Verona, P.le Scuro, 10, Verona, 37134, Italy. E-mail: emilio.pedrotti@univr.it.

Abstract

Severe ocular damage, such as corneal alkali-injury, can compromise the limbal stem cell (LSC) niches, leading to LSC deficiency (LSCD) and resulting in significant vision impairment. Current insights into the wound healing process associated with simple limbal epithelial transplantation (SLET), a therapeutic intervention for LSCD, are derived solely from clinical studies, which impose methodological limitations and hinder a complete understanding of the cellular dynamics underlying SLET. For the first time, we adapted the clinical SLET procedure to a mouse model of LSCD, enabling a robust and detailed assessment of short- and long-term morphological, immunomodulatory and cell-fate outcomes in corneal regeneration. We demonstrated that simple limbal-corneal epithelial transplantation (SLCET) treatment effectively reduces corneal opacification, vascularization, and inflammation induced by alkali-injury, with persistent benefits. We used transgenic GFP-expressing mice to isolate GFP-positive limbal-corneal cells and trace their fate in the context of SLCET. Our results revealed that both endogenous and transplanted cells contribute to replenishing the depleted limbal-corneal cell population. Furthermore, we showed that the engrafted-cells retained a long-term proliferative capacity and stemness phenotype, underscoring their role in sustained corneal regeneration. Overall, our study provides a temporal and mechanistic overview of SLCET outcomes, highlighting the engrafted-cells as key players in corneal regeneration. This framework also holds a strong translational potential for enhancing SLET's efficacy and uncovering novel LSC modulators.

Key words: SLET; LSCD; limbal-corneal stem cells; cornea regeneration.

Received: 14 April 2025; Accepted: 17 January 2026.

Graphical abstract

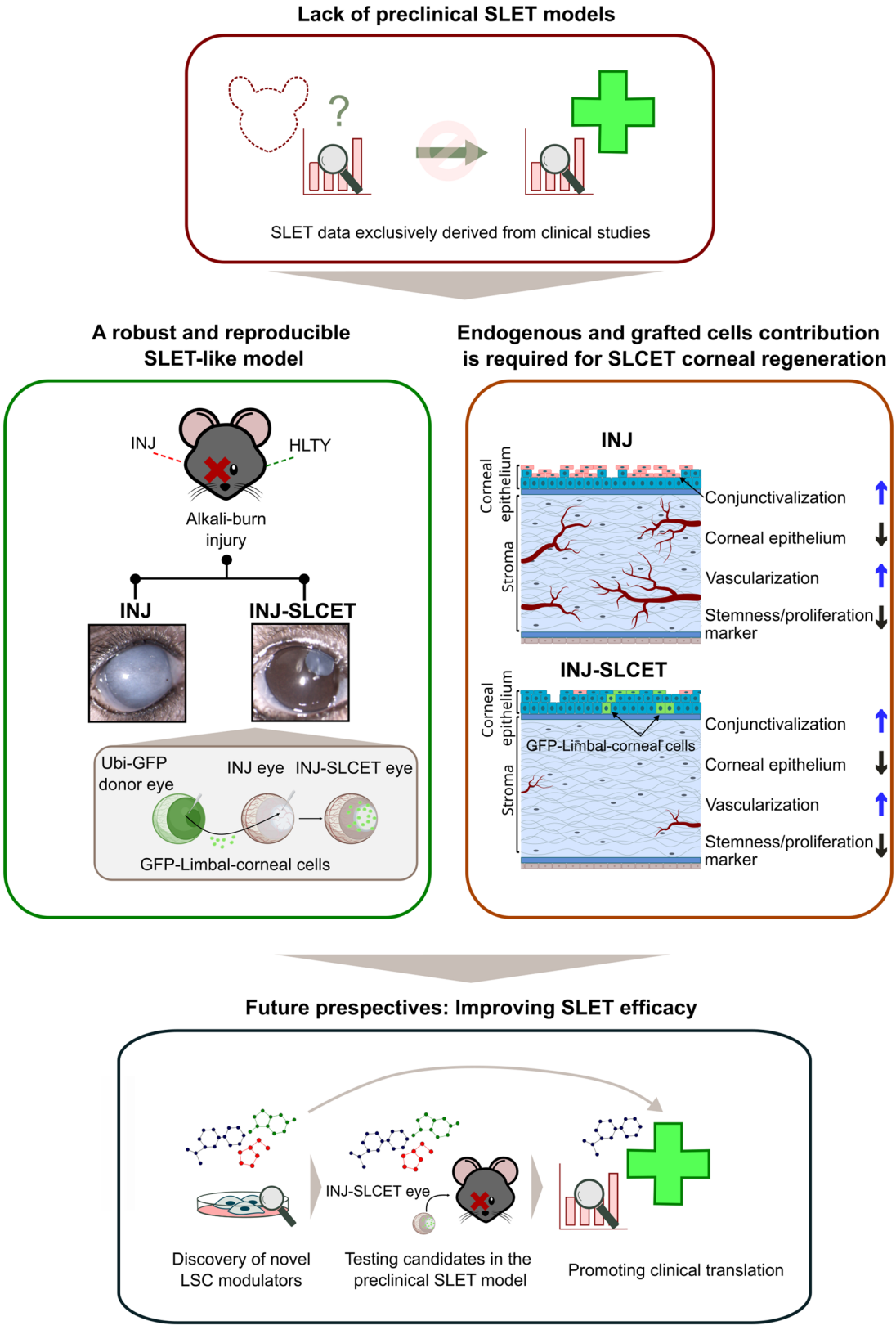

Significance statement

Simple limbal epithelial transplantation (SLET) is a clinical intervention for the loss of limbal stem cells (LSC), a painful and vision-impaired condition. Our current knowledge of SLET-driven corneal healing is exclusively derived from clinical studies and their restricted compatible methodologies. For the first time, we adapted the single-stage SLET technique to a preclinical murine model, providing an overview of corneal healing and revealing the crucial role of the transplanted cells. This framework holds a strong translational potential and sets the stage for the discovery of novel LSC modulators and further dissection of the cellular and molecular mechanisms underlying the corneal healing process.

Introduction

The corneal epithelium is the most external layer of the cornea and provides ocular protection and maintenance of the corneal transparency, crucial for vision.[1] The epithelium is continuously shredded and relies on the self-replication and migration of the limbal stem cells (LSC) for its physiological maintenance and injury recovery.[1] In the human eye, LSC reside in the Palisades of Vogt (POV), within the limbus, a region between the cornea and the conjunctiva.[2] In mice, the SC reside throughout the cornea, grouped in small islets.[3,4] Severe damage or functional disruption of the LSC niche may cause LSC deficiency (LSCD), a condition characterized by abnormal corneal healing, vascularization and conjunctivalization, visual impairment, pain, and photophobia.[5] Amniotic membrane transplantation (AMT) attenuates the inflammation and scarring induced by alkali-injury and the persistent epithelial defects detected in LSCD.[6–8]

The latest described therapeutic approach for LSCD is the simple limbal epithelial transplantation (SLET), an autograft transplantation of LSC harvested directly from the healthy eye and transplanted onto the injured eye, bypassing the need for *in vitro* culture.[9] The usage of minimal donor tissue and the lower economic impact make SLET an advantageous alternative to previous procedures.[9] Nevertheless, the cellular and molecular mechanisms involved in the SLET-driven healing process remain poorly characterized. Additionally, the long-term corneal regeneration can be negatively affected by the poor survival of the transplanted cells, a limitation prompting researchers to discover novel LSC modulators.[10] Currently, animal experimentation is focused on the transplantation of cultured cells, a setup similar to the cultivated limbal epithelial transplantation (CLET) and characterized by high economic impact.[11–13] The *in vivo* data from these studies lack a consistent and robust follow-up, with a clear and systematic characterization of the fate of the engrafted-cells regarding their stemness and differentiation potential and their ability to replenish the SC pool. Additionally, limited immunological data are available, and the impact on the functional vision is unknown. To our best knowledge, this is the first report of the short- and long-term corneal healing contributions of simple limbal-corneal epithelial transplantation (SLCET), a SLET-based approach adapted to the murine eye. We characterized the corneal regenerative contributions of the engrafted cells in a murine LSCD model and evaluated their cell fate and viability by exploiting a transgenic GFP-expressing mouse.

By adapting the single-stage technique of SLET to a preclinical model, we provided a comprehensive overview of SLCET-driven corneal healing in a clinically relevant setup, establishing a suitable model for the discovery of novel LSC modulators to enhance SLET's efficacy and to further investigate the cellular and molecular contributions underlying the healing process.

Methods

Animals

The animal housing and experimentation were approved by the National Institute of Health (I.S.S.; Istituto Superiore di Sanità, protocol 1013/2024-PR) and the Animal Ethics Committee (C.I.R.S.A.L.; Centro Interdipartimentale di Servizio alla Ricerca Sperimentale, approval 9/2022-UT) of the University of Verona (Italy). The 10-week-old wild-type C57BL/6 and Ubi-GFP C57BL/6 mice were obtained from the University of Verona's animal facility.

Study design

The study had three phases: (1) validation of the alkali-induced LSCD mouse model (Figure 1A), (2) assessing the outcomes of SLCET and AMT in the established LSCD model (Figure 2A), and (3) evaluation of the fate and specific role of the limbal-corneal cells transplanted by SLCET (Figure 3A). Only the mice's right eyes were injured, leaving the fellow eye as a healthy control (HLTY). Fifteen mice were treated via SLCET (INJ-SLCET group), 9 via AMT (INJ-AMT group), and 9 remained untreated (INJ group). For the validation of the mouse LSCD model, examinations were carried out at 4 and 9 weeks after alkali-injury, while the evaluation of SLCET and AMT treatments was carried out at 7, 21, and 40 days post-treatment (DPT).

Mouse LSCD model

We anesthetized 10-week-old C57Bl/6 mice (19 females and 14 males) with 2% isoflurane inhalation and applied a droplet of 4 mg/mL oxybuprocaine (Novesine®; Novartis, Basel, Switzerland) for local anesthesia prior to the intervention. The alkali-injury was performed as previously reported,[14] using a 7 mm diameter cotton-pad soaked in 1M NaOH for 30 s, ensuring the total corneal coverage, followed by a wash with physiologic solution. Infection and excessive pain were prevented with intraperitoneally injections of 50 mg/mL enrofloxacin (Baytril®; Bayer, Leverkusen, Germany) and 25 mg/mL carprofen (Rimadyl®; Pfizer, Manhattan, USA). The injured eye was treated daily with one droplet of 0.1% dexamethasone/0.3% netilmicin (Netildex®; SIFI, Catania, Italy) for 3 weeks.

SLCET and AMT in a mouse LSCD model

Three weeks post-injury, mice anesthetized with 4-5% isoflurane and maintained under 2% underwent SLCET and AMT surgeries. For SLCET surgery, after pannectomy via crescent knife, a 3 mm cryopreserved, intact AM with the epithelial side up was glued on the injured eye with a minimum amount of fibrin glue (Tisseel, Baxter, AU) (**Supplementary Material S1 and Video**). Since putative corneal SC exist throughout the murine cornea, with indistinguishable proliferative potential between the limbal and corneal epithelium,[3] both healthy eyes

of 5 C57Bl/6 mice were submitted to a complete limbal-corneal epithelial debridement by scraping the entire cornea for cell harvesting. Those cells were glued on the AM, avoiding a glue excess, following standard practices.[9] The INJ-AMT group underwent pannectomy and AM transplantation by fibrin glue, without engraftment. The eyelids were closed with a single-point suture to avoid injuries or membrane removal. Each mouse donated cells to two recipient mice that underwent SLCET. To minimize the usage of genetically modified strains, 3 Ubi-GFP C57Bl/6 mice were used as donors only in the last subset of experiments. The transplantation was done similarly to the wild-type strain. From the first day post-surgery until the day of sacrifice, Netildex® was topically administered. The animals were sacrificed by cervical dislocation.

Slit-lamp examination and fluorescein staining

Slit-lamp microscope examination was performed to assess the condition of the ocular surface in the LSCD model and after the SLCET and AMT. The presence of neovascularization, corneal opacity, and both early and late fluorescein staining were evaluated according to standard practices.[15]

In vivo confocal microscopy (IVCM)

IVCM (HRT3, Rostock Cornea Module, Heidelberg Engineering, Dossenheim, Germany) was performed to assess the epithelium phenotype on the corneal surface and the presence of inflammatory and goblet cells.[15]

Immunofluorescence

The eyeballs were removed and fixed overnight in 4% PFA/4% sucrose at 4 °C, rinsed in PBS 1X and stored in 30% sucrose/PBS solution at 4 °C. Sagittal cryosections of 20 µm thickness were obtained and stored at −20 °C. Before the immunostaining, the sections were incubated in blocking solution (BS; PBS 1X with 0.25% Triton X-100, 2% Bovine Serum Albumin) for 30 min at room temperature (RT). Primary antibody solutions were prepared in BS at the appropriate dilution (Table 1) and incubated overnight at 4 °C. Next, the sections were rinsed 6 times for 5 min in BS, and the appropriate secondary antibodies were incubated for 4 h at RT. When multiplexing antibodies from the same host, a fluorophore-conjugated primary antibody was used. Finally, the section was rinsed 3 times for 5 min in BS and another 3 times for 5 min in PBS 1X before counterstaining the nucleus with 1:3,000 TO-PRO™-3 Iodide (TO-PRO-3, Molecular Probes-Thermo Fisher Scientific) for 10 min. The slices were mounted using 1,4-Diazabicyclo [2.2.2] octane (DABCO, Sigma-Aldrich).

RNAscope

Corneal sections of 10 µm thickness, mounted onto Superfrost™ Plus slides (Epredia, J1800AMNZ, New Hampshire, USA), were allowed to reach RT, rinsed in PBS, and baked for 30 min at 60 °C in the HybEZ™ Oven (Advanced Cell Diagnostics [ACD], Minnesota, USA). Sections were post-fixed with 4% PFA for 10 min, followed by dehydration in an ethanol gradient (50%, 70%, and twice in 100%; 5 min each) and air-dried. Next, pretreatment with hydrogen peroxide (ACD, 322335) for 10 min, set at 98–102 °C in target-retrieval solution (1X; ACD, 323165), followed by treatment with protease-plus (ACD, 322331) at 40 °C for 30 min in the HybEZ™ Oven, was performed.

Table 1. Primary and secondary antibodies used for immunofluorescence.

Primary antibodies			
Target	**Host**	**Working dilution**	**Manufacture**
ABCG2	Rat	1:200	24115, Abcam
CD31	Rat	1:400	557377, BD Biosciences
GFP 488-conjugated	Rabbit	1:500	A21311, Invitrogen
Iba1	Rabbit	1:200	019-19741, WAKO
Keratin 12 (K12)	Guinea pig	1:200	AP09545SU-N, Origene
Keratin 14 (K14)	Mouse	1:200	7800, Abcam
Keratin 19 (K19)	Rabbit	1:200	Ab52625, Abcam
Ki67	Rabbit	1:200	Ab16667, Abcam
Laminin	Rat	1:200	NBP1-51759, Novus Biologicals
Nestin	Mouse	1:200	MAB2736, R&D systems
deltaNp63 (p63)	Rabbit	1:800	67825, Cell signaling
Secondary antibodies			
Target	**Host**	**Working dilution**	**Manufacture**
Anti-guinea pig Alexa Fluor® 594	Donkey	1:1000	Jackson ImmunoResearch
Anti-mouse Alexa Fluor® 488	Donkey	1:1000	Invitrogen
Anti-mouse CY™ 3	Goat	1:1000	Amersham
Anti-rat CY3	Donkey	1:1000	Jackson ImmunoResearch
Anti-rabbit Alexa Fluor® 488	Donkey	1:1000	Invitrogen
Anti-rabbit Alexa Fluor® 546	Donkey	1:1000	Invitrogen

Before RNAscope analysis, slides were immunostained with anti-GFP antibody, as previously described, and the bound antibodies were post-fixed in 4% PFA for 30 min prior to RNAscope processing. RNA hybridization with the Mm-KRT12 probe (ACD, 523671) for 2 h at 40 °C, followed by two washes of 2 min in RNAscope wash buffer (1X; ACD, 310091), was done. Signal amplification was performed with the RNAscope Multiplex Fluorescent Detection Kit-v2, using sequential incubation with Amp-1 (30 min, 40 °C), Amp-2 (30 min, 40 °C), and Amp-3 (15 min, 40 °C). Signal was developed by applying HRP-C1 for 15 min at 40 °C, followed by incubation with Opal-690 (1:200 in TSA-buffer; Akoya Biosciences, San Francisco, USA, FP1497001KT) for 30 min and HRP-Blocker for 15 min. Slides were washed twice in 1X wash buffer (2 min) after each step. Nuclei were counterstained with DAPI, and slides were mounted with ProLong™ Gold Antifade Mountant (Thermo Fisher Scientific, 2801574).

Image acquisition and quantification

Immunofluorescent images were acquired with 200× and 300× magnification on a FLUOVIEW™ FV4000 confocal microscope (Evident, Tokyo, Japan) and on a Nikon Ti1 fluorescent microscope (Nikon Corporation, Tokyo, Japan), with identical acquisition parameters for all conditions. Marker expression was quantified on ImageJ software (http://rsb.info.nih.gov/ij/, ImageJ bundled with 64-bit Java 8), using at least 5 images from at least 3 different mice per experimental group. Briefly,

total corneal nuclei, as well as basal, wing, and superficial cells, were manually counted using the cell-counter plugin. Threshold adjustment was done to define the region of interest and determine the K12$^+$- (corneal marker),[16] K19$^+$- (conjunctive marker),[17] CD31$^+$-area and laminin$^+$-area (vessel markers),[18,19] for at least five 400 µm sections of each sample. The thickness of the K12$^+$-corneal epithelium and of the stroma was determined by performing 3 measurements in each 400 µm section. The number of K12$^+$-, K14$^+$-,[20] deltaNp63$^+$-,[21] ABCG2$^+$-[22] (putative corneal stemness markers), Ki67$^+$- (proliferation marker), Nestin$^+$- (stemness marker)[23] and GFP$^+$-cells were determined through manual counting of the positive cells in the corneal epithelium. Attending to the murine and human corneal differences, particularly the absence of the POV,[3] the unprecise identification of the limbal epithelium in sagittal cuts,[24] and the indistinguishable regenerative capacity between the mouse's peripheral and central corneal epithelium,[3,25] the analyses were carried out at the central cornea and only at the peripheral (i.e., vicinity of the conjunctival epithelium, above the ciliary body, containing the limbus) when indicated.

Assessment of the visual function

Murine's visual function assessment was performed using four Touchscreen-equipped Operant Chambers (TOCs) (Campden Instruments Ltd., Leicestershire, UK) (**Figure S2E**). Each TOC was equipped with an LED house light for IR illumination, a touchscreen on the front, and a liquid tray on the rear. A peristaltic pump provided 12.8% strawberry-flavored condensed milk solution as a reward contingently to correct responses. Apart from two equally sized response windows, the touchscreen was covered by a plastic mask to reduce accidental touches. Each chamber was encased in a sound-insulated cubicle, equipped with a ventilation fan, a tone generator, and an IR video camera (**Figure S2D**). Stimuli display and data recording were controlled by ABET II software (Campden Instruments Ltd., Leicestershire, UK).

Animals were housed in an inverted light/dark cycle condition, with *ad libitum* water and food restriction to 85-90% of their *ad libitum* intake, and trained to perform pairwise discrimination, during which the mouse was simultaneously exposed to two different stimuli, i.e., a plane and a spider (**Figure S2E**). Half of the mice had the plane associated with the reward delivered contingently to a tone (1 s, 3 kHz) and no reward with a 5 s-delay punishment associated with the spider, and vice-versa for the second half. Between two consecutive trials, mice had to wait for 20 s. The discrimination task was considered acquired when the mice reached 80% of correct responses over 30 trials for two consecutive sessions. The test was run for 11 weeks, with 2 sessions occurring prior-to-injury (performance baseline), 2 post-injury and prior-to-treatment, and 7 sessions post-treatment. Twenty-four hours prior-to-test, the healthy eye was temporarily closed with a one-point suture to block the vision.

Statistical analysis

Statistical analysis and graphical representation were done with GraphPad Prism 9 (GraphPad Inc., La Jolla, CA). Multiple comparisons between normally distributed data sets were done by one-way ANOVA, followed by Sidak's or Tukey's post hoc test. Comparison between two datasets was done by Student's *t*-test. A *P*-value ≤.05 was considered statistically significant. The exact statistical test used to generate each *P*-value is indicated in the respective figure caption.

Results

Alkali-burn model closely resembled the LSCD condition

To setup a LSCD murine model, we induced an alkali-injury on the right eye of 10-week-old mice, keeping the non-injured left eye as healthy control. We then evaluated the short- (4 weeks) and long-term (9 weeks) outcomes (Figure 1A) by comparing the cornea integrity, thickness, conjunctivalization, vascularization, and stemness between the injured (INJ group) and the healthy eyes (HLTY group). At 4 weeks post-injury, slit-lamp examination revealed corneal opacification, vascularization and early fluorescein staining, in contrast with the clear cornea of HLTY eyes (Figure 1B, black arrows). The analysis at 9 weeks confirmed the loss of corneal integrity and a progressive corneal degeneration with involvement of the eyelids, closely resembling the typical ocular injury of LSCD patients (Figure 1B).

The eyes were sectioned to assess the corneal morphological composition by immunofluorescence. A significant reduction to 0.77 ± 0.04-fold change of the epithelial nuclei occurred at 4 weeks post-injury (Figure 1C and G). The progressive degeneration detected by slit-lamp was associated with a significant aggravation of the corneal nuclei loss to 0.57 ± 0.05-fold change at 9 weeks. The healthy corneal epithelium presents 3 cell populations: superficial, wing, and basal cells.[26] At 4 weeks post-injury, the number of basal cells significantly reduced from 252.04 ± 10.20 (HLTY) to 194.72 ± 8.90 (INJ group). Further reduction was found at 9 weeks, from 271.39 ± 1.82 (HLTY) to 137.99 ± 17.47 (INJ). In the long-term, the number of the wing cell population also decreased from 345.44 ± 16.79 (HLTY) to 162.50 ± 35.00 (INJ). In line with these observations, the percentage of corneal K12$^+$-cells significantly reduced to 0.353 ± 0.101-fold change at 4 weeks (Figure 1D and I). At 9 weeks, K12$^+$-cells further decreased to 0.148 ± 0.044-fold change (INJ), while the HLY group had a small non-significant reduction to 0.673 ± 0.045-fold change. Additionally, the corneal epithelial thickness decreased to 0.59 ± 0.06-fold change (Figure 1D and J) at 4 weeks post-injury and remained significantly lower (0.43 ± 0.06) than the HLTY group (0.73 ± 0.02) at 9 weeks. These results suggested a progressive disruption of corneal structure in the INJ group.

The alkali-injury markedly contributed to the increase of K14$^+$-cells and K14$^+$/K12$^+$-cells to 5.88 ± 1.47-fold change in the peripheral (including the limbus) and 13.92 ± 1.99-fold change in the central epithelium, relative to the HLTY group at 4 weeks (Figure 1E and K; **Figure S1A**). In the INJ group, the K14-expressing cells remained elevated at 9 weeks, with a 7.633 ± 2.15-fold change in the peripheral epithelium and a 14.91 ± 0.56-fold change in the central.

The corneal opacification detected by slit-lamp correlated with the extensive conjunctivalization assessed by K19$^+$-area (21.98 ± 2.86-fold change and 13.94 ± 1.54-fold change relative to the HLTY group, at 4 and 9 weeks, respectively; Figure 1F and L). Additionally, a significant increment in the stromal vascularization to 12.70 ± 2.74-fold change was detected at 4 weeks (Figure 1M and N), expressed as stromal

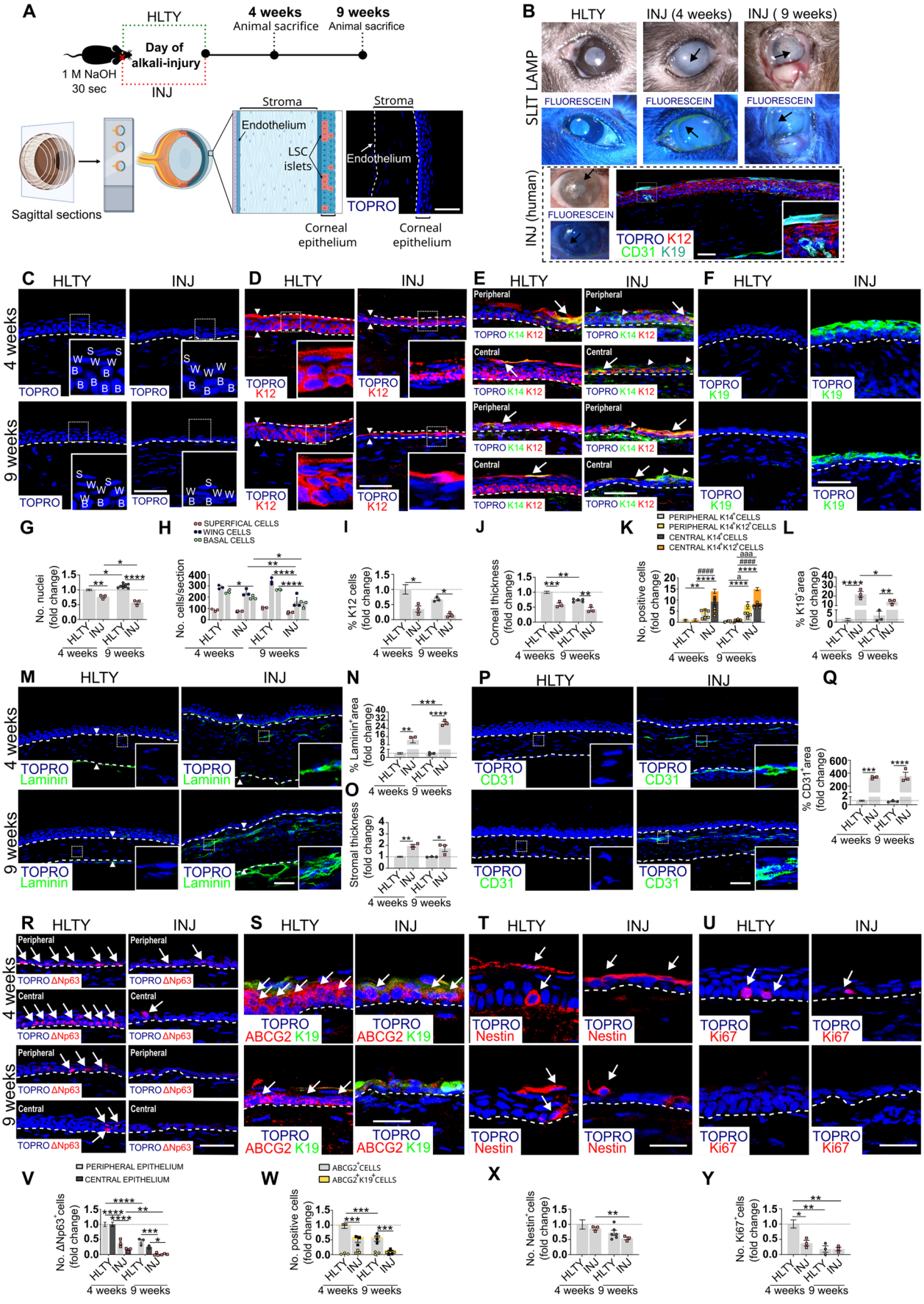

Figure 1. Validation of the alkali-burn as a model of limbal stem cell deficiency (LSCD). (A) Diagram of alkali-induced LSCD mouse model. The alkali-burn was performed on the right eye (injured group; INJ), leaving the non-injured left eye as a healthy control (HLTY). Post-injury outcomes were assessed at 4 and 9 weeks in the corneal epithelium or stroma of 20 μm thick sagittal sections using different markers. (B) Representative images of slit-lamp

laminin$^+$-area. Injury progression exacerbated the corneal vascularization, leading to a significant 29.17 ± 1.50-fold change increase in laminin$^+$-area, at 9 weeks (Figure 1N). The stromal thickness was also evaluated as a hallmark of corneal injury.[27,28] At 4 weeks, stromal thickness increased to 1.96 ± 0.12-fold change, an increment maintained at 9 weeks (Figure 1O). The neovascularization was further confirmed by the increase in CD31$^+$-area to 333.0 ± 11.32 (4 weeks) and 355.2 ± 58.33-fold change (9 weeks, Figure 1P and Q).

The corneal stemness profile was assessed by Nestin (stemness), Ki67 (proliferation), deltaNp63, and ABCG2 expressions (LSC putative markers). At 4 weeks, the deltaNp63$^+$-cells were severely depleted in both the peripheral and central cornea, to 0.36 ± 0.07 and 0.17 ± 0.03-fold change, respectively (Figure 1R and V; Figure S1B). The initial LSCD was estimated at 63.62%, as the percentage of lost peripheral deltaNp63$^+$-cells, relative to the healthy eye. Lesion progression nearly ablated the deltaNp63-expressing cells in the INJ group, in the peripheral (0.02 ± 0.02-fold change) and central cornea (0.01 ± 0.01-fold), suggesting a total LSCD at 9 weeks post-injury. A significant age-related reduction to 0.44 ± 0.06-fold change of the peripheral deltaNp63$^+$-cells was observed in the HLTY group. The ABCG2/K19 expression was analyzed in the peripheral cornea, due to their poor expression in the central healthy cornea at 9 weeks. The ABCG2$^+$-cells significantly reduced to 0.59 ± 0.0318-fold change, at 4 weeks (Figure 1S and W; Figure S1C). Similarly to the deltaNp63 expression, the loss of ABCG2$^+$-cells was more severe over time, reaching 0.163 ± 0.024-fold change. The injury progression also showed a significant reduction of the Nestin$^+$-cells in the INJ group from 0.87 ± 0.05-fold change (4 weeks) to 0.54 ± 0.05-fold (9 weeks, Figure 1T and X; Figure S1D). Regarding the proliferative properties, the number of Ki67$^+$-cells significantly reduced to 0.38 ± 0.09-fold-change at 4 weeks (Figure 1U and Y; Figure S1E). The drastic decrease of Ki67$^+$-cells of nearly 80% in both groups, at 9 weeks, suggested a time-dependent alteration of the proliferative properties not associated with the alkali-injury.

The presented alkali-injury model successfully mimicked the abnormal corneal healing observed in LSCD patients, such as (i) the loss of corneal integrity and thickness, (ii) the development of corneal conjunctivalization and stromal neovascularization,[29] (iii) interchange of corneal-specific keratins (e.g., K12$^+$) by conjunctive-specific keratins (e.g., K19$^+$), and (iv) the impairment of the proliferative and stemness potential, extensively reported by others.[13,30,31]

SLCET improves corneal regeneration in the LSCD mouse model

We comprehensively assessed the therapeutic efficacy of SLCET by combining confocal clinical imaging, immunofluorescence evaluations of neovascularization, inflammation, and corneal cell composition, and functional vision outcomes. The corneal healing outcomes following SLCET (INJ-SLCET group) were evaluated at 7, 21, and 40DPT, and compared against AMT (INJ-AMT group) and untreated INJ controls (Figure 2A).

Under slit-lamp examination, the INJ group showed a symblepharon, a condition in which the bulbar and palpebral conjunctivae abnormally adhere to each other,[32] the presence of stromal blood vessels, and corneal opacity with extensive fluorescein staining (Figure 2B). At 40DPT, INJ-AMT and INJ-SLCET presented a translucent cornea and absence of symblepharon. However, while fluorescein staining and some peripheral blood vessels were found in INJ-AMT, they were undetectable in the INJ-SLCET group. Visual comparison with a patient after SLET (Figure 2B) revealed close similarities between the preclinical and clinical observations.

IVCM examination showed a lack of corneal epithelium, presence of blood vessels, dendritic and goblet cells, and conjunctival epithelium in the INJ group at all follow-ups (Figure 2B, black arrows). The INJ-AMT group presented an unstructured layer where the membrane was still present and a conjunctival epithelium with few signs of inflammation, once the membrane had been reabsorbed. In the INJ-SLCET group, islands of corneal epithelium and immature cells were identified (Figure 2B, asterisk), suggesting corneal regeneration.

SLCET significantly reduced vascularization, as demonstrated by decreased laminin+-area (0.01 ± 0.01 mm^2 vs. INJ: 0.08 ± 0.02 mm^2 at 7DPT; Figure 2C and E) with long-lasting

examination and fluorescein staining of a mouse cornea. An example of the pathological alterations in an LSCD patient is provided. Black arrows indicate corneal opacity and vascularization in the INJ eyes. (C) The corneal injury was assessed by the number of corneal epithelial nuclei, using the nuclear marker TO-PRO™-3 (blue). The inserts detailing the different corneal populations (S: Superficial cells; W: Wing cells; B: Basal cells). (D) The corneal epithelium thickness was defined by the keratin-12$^+$ area (K12, red, delimited by dashed lines). Opposing arrowheads provide a visual aid of the corneal thickness. Inserts provide a digital magnification. (E) Representative confocal images of K14$^+$ (green) and K12$^+$-cells (red) in the corneal epithelium showing the increase of single K14$^+$ (arrowheads) and double K14$^+$/K12$^+$ cells (arrows), after the alkali-burn. (F) The corneal conjunctivalization was evaluated as keratin-19$^+$-area (K19, green) in the corneal epithelium. (G) Graph showing the fold change post-injury reduction of the number of nuclei. (H) Graph expressing the number of different corneal populations. (I) Graph representing the fold change reduction of K12$^+$-cells following the alkali-burn. (J) Graph representing the fold change decrease in corneal epithelium thickness. (K) Graph expressing the fold change increase in K14$^+$- and K14$^+$/K12$^+$-cells in the peripheral and central corneal epithelium following alkali-burn. (L) Graph representing the fold change increase in corneal conjunctivalization. The y-axis is shown split. (M) Representative confocal images of the stromal vascularization (Laminin$^+$-area, green) following alkali-burn. White arrowheads limit the stroma thickness. Inserts provide a digital magnification. (N) Graph showing the fold change increase of stromal Laminin$^+$area. The y-axis is presented split. (O) Graph showing the fold change increase of the corneal stroma thickness in the INJ group. (P) Representative confocal images of the stromal vascularization following alkali-burn, measured as CD31$^+$-area (green). Inserts provide a digital magnification. (Q) Graph showing the fold change increase in CD31$^+$area in the stroma. (R) Representative confocal images of deltaNp63$^+$-cells (red, white arrows) in the peripheral and central corneal epithelium. (S) Representative confocal images of ABCG2$^+$ (red, white arrows) and K19$^+$-cells (green) in the peripheral corneal epithelium. ABCG2 and K19 were tendentially mutually exclusive. (T) Representative confocal images of Nestin$^+$-cells (red, white arrows) in the corneal epithelium. (U) Representative confocal images of Ki67$^+$-cells (red, white arrows) in the corneal epithelium. (V) Graph showing the fold change decreasing in deltaNp63$^+$-cells in the corneal epithelium. (W) Graph showing the fold change decreasing in ABCG2$^+$-cells in the peripheral corneal epithelium. (X) Graph showing the fold change decreasing trend of corneal Nestin$^+$-cells. (Y) Graph representing the fold change decrease in Ki67$^+$-cells in the corneal epithelium following alkali-burn. The peripheral corneal epithelium comprises the limbal cornea. Scale bar: 50 µm (A-F, M, and P) or 25 µm (R-U). Data were expressed as fold change relative to the HLTY group at 4 weeks post-injury and plotted as mean ± SEM (one-way ANOVA with Sidak's post–hoc test and two-tailed *t*-test in case of (Y); at least 3 biological repeats). **P*-value <.05, ***P*-value <.01, ****P*-value <.001, *****P*-value <.0001 vs the indicated groups. ####*P*-value <.0001 vs single positive cells of the indicated groups. ^{a}*P*-value <.05, ^{aaa}*P*-value <.001 vs double positive cells of the indicated groups.

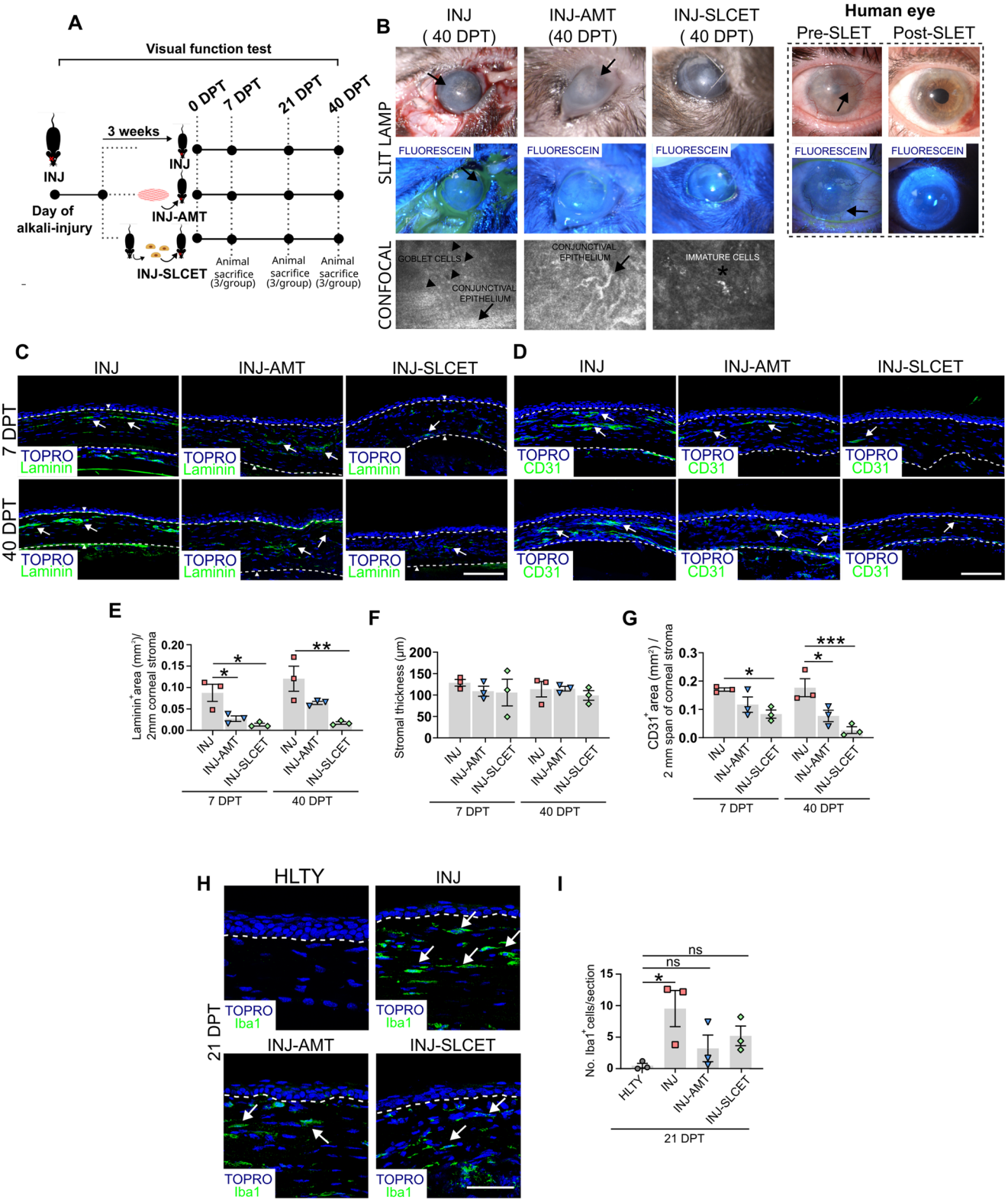

Figure 2. Simple limbal-corneal epithelial transplantation (SLCET) contributed to a robust and sustainable reduction of corneal vascularization and modulated the cellular immune-response after alkali-burn. (A) Diagram of SLCET in a murine model of limbal stem cell deficiency (LSCD). Alkali-burn was performed on the right eye, and the mice were divided into 3 experimental groups, 3 weeks after injury. One group underwent amniotic membrane application (INJ-AMT), another group was submitted to SLCET procedure (INJ-SLCET), and the last group was left untreated (injured group; INJ). Animals were sacrificed at 7 and 40 days post-treatment (DPT) to analyze the injury recovery, and at 21DPT to assess the immune-response outcome. Assessment of the visual function was carried out throughout the entire experiment. (B) Representative images of slit-lamp examination, with and without fluorescein staining, and *in vivo* confocal microscopy (IVCM) of the mouse cornea, at 40DPT. An example of the clinical outcomes in a patient 3 months post-SLET is additionally presented. Black arrows indicate corneal opacity and corneal disruptions (detected with fluorescein). IVCM images show a lack of corneal epithelium and presence of blood vessels, goblet (arrowheads) and dendritic cells, and conjunctival epithelium in the INJ group and

effects (0.02 ± 0.01 mm² vs. INJ: 0.12 ± 0.03 mm² at 40DPT). CD31 quantification confirmed this trend at both timepoints (Figure 2D and G). AMT had only partial anti-angiogenic effects (Figure 2C–G). Stromal thickness remained unchanged across groups (Figure 2F).

To investigate if SLCET modulated the injury-induced inflammatory response, we evaluated the stromal Iba1⁺-macrophages infiltration at 21DPT. As expected, the INJ group had a significant increase in Iba1⁺-cells (9.5 ± 1.72), whereas the stromal macrophages were essentially absent from the healthy eyes (0.47 ± 0.24, Figure 2I). Both INJ-AMT (3.5 ± 1.22) and INJ-SLCET (5.2 ± 0.89) groups showed a non-significant trend to reduce the macrophage infiltration (Figure 2H and I), suggesting a potential immunomodulatory effect.

We next evaluated corneal epithelial recovery. The number of nuclei significantly increased in the INJ-SLCET group (102.7 ± 4.30) compared to the INJ (73.89 ± 6.85), at 40DPT (Figure 3A and E) with no statistical differences among relative contribution of superficial, wing and basal corneal epithelial populations (Figure 3F). The percentage of K12⁺ corneal-specific keratin cells was significantly increased in the INJ-SLCET group (60.10 ± 4.77%) compared to both INJ (23.32 ± 6.65%) and INJ-AMT groups (33.86 ± 6.13%), at 7DPT (Figure 3B and G). Consistently, RNAscope qualitative analysis (Figure S2A) showed higher levels of K12 transcripts in the INJ-SLCET. Despite the general loss at 40DPT, the amount of K12⁺-cells remained significantly higher in the INJ-SLCET group (Figure 3G). The corneal thickness was significantly larger in the INJ-SLCET group (20.87 ± 0.75 µm) compared to INJ group (15.64 ± 1.48 µm), only at 7DPT (Figure 3B and H). These transient changes were not associated with post-SLCET cell clumps, which were undetected at any timepoint (Figure S2B). SLCET strikingly attenuated the corneal conjunctivalization, significantly reducing the corneal K19⁺-area (9.55 ± 0.57%), at 7DPT, relatively to the INJ group (27.42 ± 3.56%; Figure 3C and I) with this beneficial effect persisting long-term (INJ-SLCET: 6.23 ± 2.25% and INJ: 17.39 ± 1.92%). These results indicated that SLCET promotes corneal epithelial restoration following alkali-injury.

Next, we evaluated the presence of limbal-corneal progenitors cells expressing the putative limbal-corneal stem cell markers deltaNp63, ABCG2 and K14. Despite both AMT (19.45 ± 2.41) and SLCET treatment (21.66 ± 4.17) had contributed to significantly increase the number of deltaNp63⁺-cells relatively to the INJ group (6.45 ± 2.00), at 7DPT (Figure 3D and J; Figure S2C), only SLCET (20.52 ± 1.87) contributed to the long-term replenishment of the deltaNp63⁺-population (INJ: 0.47 ± 0.09, INJ-AMT: 1.57 ± 0.44). Similarly, INJ-SLCET had significantly more ABCG2⁺-cells (28.10 ± 2.869) than the INJ (17.77 ± 0.984) and AMT groups (17.63 ± 1.462), at 7DPT (Figure 3K and M; Figure S2D). While in the INJ (5.00 ± 0.764) and INJ-AMT groups (4.17 ± 0.593) the ABCG2⁺-cells got further reduced with injury progression, this population was partially maintained in the INJ-SLCET group (12.83 ± 1.256). The K14 expression strengthened SLCET's contribution in recovering the physiological corneal state. Specifically, at 7DPT, all groups presented a high number of K14⁺-cells in the peripheral (INJ: 19.20 ± 4.81, INJ-AMT: 12.93 ± 1.29, INJ-SLCET: 24.40 ± 2.60) and central cornea (INJ: 21.37 ± 3.03, INJ-AMT: 17.27 ± 2.20, INJ-SLCET: 17.00 ± 3.04; Fig 3L, 3N and Figure S2B). While at 40DPT, the K14⁺-cells prevailed increased in the INJ group (peripheral: 24.93 ± 7.00 and central: 22.87 ± 0.87), they decreased in the INJ-SLCET (peripheral: 5.40 ± 1.04 and central: 2.90 ± 0.97). The AMT only moderately reduced the K14 expression (peripheral: 11.67 ± 7.20 and central: 11.67 ± 7.20). Overall, our data demonstrated that SLCET contributed to preserve the limbal-corneal progenitor population after alkali-injury.

We then assessed, in a pairwise discrimination test, SLCET visual discrimination functional outcomes. After injury, the percentage of correct responses decreased from 76.58 ± 3.25% (prior-injury) to 56.09 ± 3.84% (post-injury), indicating a loss in the discrimination ability (Figure 3O). The animal's weight was similar among the groups throughout the experiment (Figure S2F). Post-treatment changes in the visual discrimination were assessed by the average of the % of correct trials from the last two sessions before animal sacrifice (sessions 10 and 11, Figure S2F). Only the INJ-SLCET group showed a significant improvement (76.61 ± 4.98%) compared to the post-injury baseline, while the INJ (56.52 ± 4.28%) and the INJ-AMT (65.84 ± 3.50%) scored lower. This finding was strengthened by the moderated inverse correlation between corneal K19 expression, associated with corneal conjunctivalization and opacity,[33,34] and the % of correct trials (Figure 3P).

Collectively, these data suggested that SLCET, but not AMT, improved the post-injury corneal healing by significantly decreasing the corneal vascularization and conjunctivalization, increasing the corneal progenitor and keratin cells, and improving the visual discrimination.

Engrafted and endogenous cells directly contribute to restore the corneal epithelium

To assess the fate and the specific role of engrafted cells in replenishing or stimulating the proliferative and stemness of endogenous cells, Ubi-GFP C57Bl/6 mice were used as donors for SLCET (Figure 4A) and the GFP⁺-cells were transplanted into the alkali-injured eyes (Figure 4B).

The number of engrafted and endogenous K12⁺-cells was determined. The INJ-SLCET group showed a statistical increase in K12⁺-cells (19.26 ± 0.672) compared to the INJ (10.0 ± 0.807) and INJ-AMT groups (8.27 ± 2.10) at 7DPT, an increment maintained in the long-term (INJ: 6.68 ± 1.58; INJ-AMT: 8.57 ± 1.15; INJ-SLCET: 13.22 ± 1.02) (Figure 4C and D). The long-term maintenance of the corneal phenotype occurred with a significant increment of the K12⁺-cells among the

conjunctival epithelium with few signs of inflammation in the INJ-AMT group (black arrows). Islands of corneal epithelium and immature cells were detected in the INJ-SLCET group (black asterisk). (C) Stromal vascularization was evaluated using the vessel marker Laminin (green; white arrows). Dash lines limit the stroma area. White arrowheads provide a visual aid of the stroma thickness. (D) Stromal vascularization was evaluated using the endothelial marker CD31 (green; white arrows). Dash lines limit the stroma area. (E) The graph expresses the Laminin⁺-area measured over a 2 mm span of corneal stroma. (F) Graph showing the corneal stroma thickness. (G) Graph expressing the CD31⁺-area measured over a 2 mm span of corneal stroma. (H) Representative confocal images showing the stromal macrophages infiltration (Iba1⁺-cells, green, white arrows), at 21DPT. (I) Graph showing the increase in the number of Iba1⁺ cells following alkali-burn. Scale bar: 100 µm (C, D) or 50 µm (F). Data are plotted as mean ± SEM (One-way ANOVA with Sidak's post-hoc test; $N = 3$). **P*-value <.05, ***P*-value <.01, *P*-value <.001, ns, non-significant.

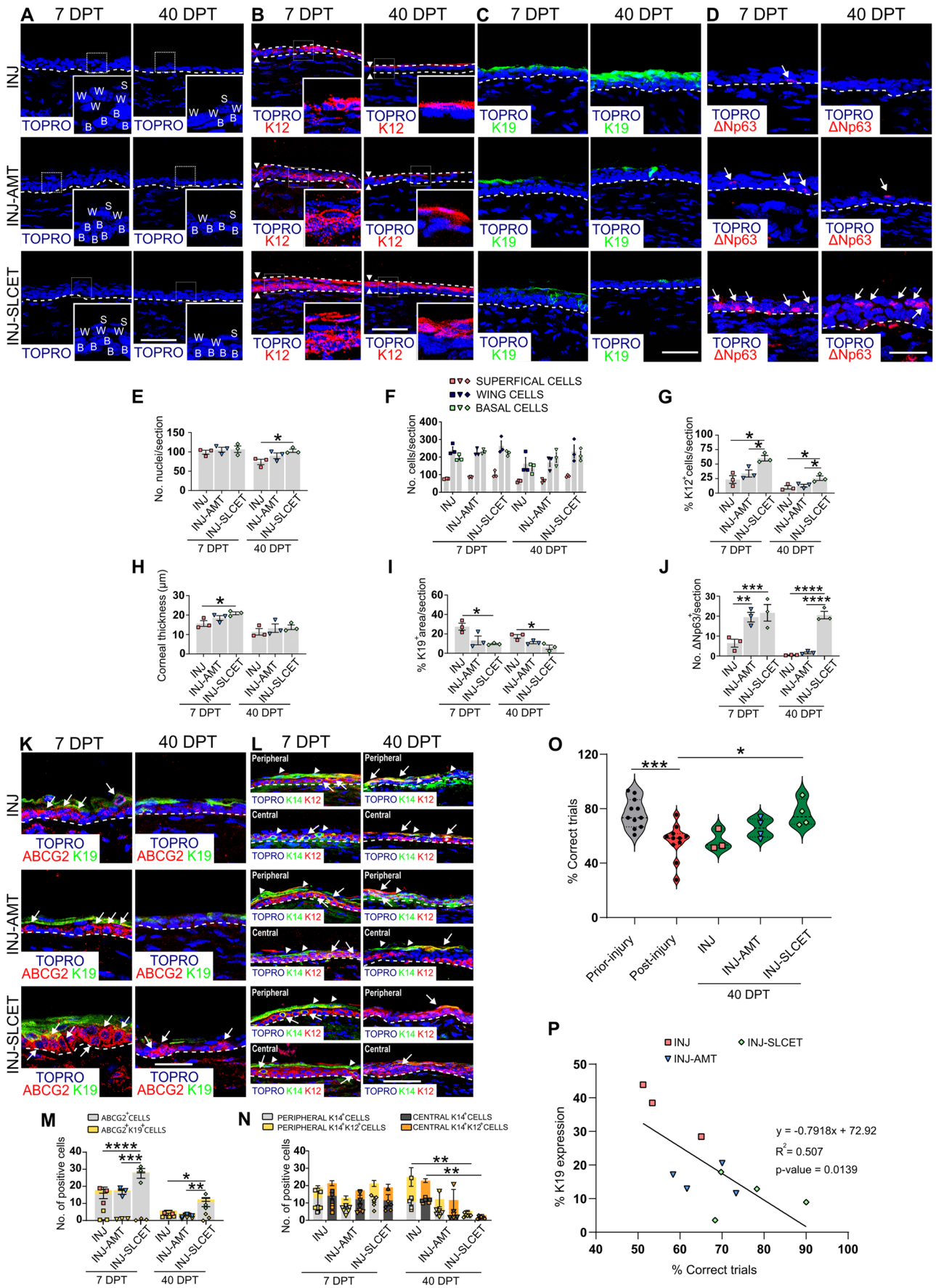

Figure 3. Simple limbal-corneal epithelial transplantation (SLCET) contributed to a robust and sustainable reduction of corneal conjunctivalization and recovery of the corneal phenotype. (A) The number of corneal epithelial nuclei was determined using the nuclear marker TO-PRO™-3 (blue) in the different experimental groups. The inserts detailed the different corneal populations (S: Superficial cells; W: Wing cells; B: Basal cells). (B) Keratin-12+

engrafted-cells in the INJ-SLCET group (7DPT: 70.9 ± 4.85%, 40DPT: 88.6 ± 3.10%; Figure 4E).

At 7DPT, the AMT (2.73 ± 0.41) and SLCET groups (2.70 ± 0.39) showed a non-significant higher number of Ki67$^+$-cells than the INJ group (1.47 ± 0.21; Figure 4F and G). The Ki67$^+$-cells became further reduced in INJ (0.74 ± 0.14) and INJ-AMT groups (1.14 ± 0.53), at 40DPT, whereas their presence increased in the INJ-SLCET (3.37 ± 0.52; Figure 4G) by expansion of the engrafted cell population. While the endogenous (GFP$^-$) Ki67$^+$-cells remained stable over time, the GFP$^+$/Ki67$^+$-cells nearly doubled between timepoints (7DPT: 22.3 ± 6.3%, 40DPT: 55.2 ± 5.69%; Figure 4H), suggesting persisting proliferative properties among the engrafted cellular population.

Additionally, the INJ-SLCET group (11.70 ± 0.71) showed a significantly higher number of Nestin$^+$-cells compared to INJ (8.40 ± 0.45) and INJ-AMT groups (7.00 ± 0.50) at 7DPT and 40DPT (INJ: 5.20 ± 0.44; INJ-AMT: 4.20 ± 0.17; INJ-SLCET: 6.83 ± 0.45; Figure 4I, J), suggesting a replenishment of the corneal SC pool in the INJ-SLCET group. The majority of the transplanted GFP$^+$-cells were Nestin-expressing cells, at 7DPT (77.6 ± 3.68%; Figure 4K), and retained a long-term stemness potential, as indicated by a non-significant increase of the Nestin$^+$/GFP$^+$-cells (91.3 ± 4.03%), at 40DPT.

The transplanted GFP$^+$-cells were evenly distributed across the peripheral (7DPT: 7.03 ± 0.717, 40DPT: 10.06 ± 0.845) and central corneal epithelium (7DPT: 5.77 ± 0.524, 40DPT: 9.80 ± 0.315; Figure 4L and 4M), suggesting no preferential location at any timepoint. Moreover, although the amount of transplanted putative SC, i.e. deltaNp63$^+$-cells, was relatively low (7DPT: 29.38%, 40DPT: 17.18%; Figure 4N), there was no statistical evidence of this cell population being sloughed-off during the timeframe of the study. Overall, our results indicated that endogenous and engrafted-cells participated in restoring the corneal epithelium following alkali-injury.

Discussion

SLET, an innovative therapy for LSCD, requires minimal donor tissue and has a low economic impact.[9] Currently, *in vivo* experimentation is focused on the transplantation of cultured stem and progenitor cells (CLET-based techniques), making our knowledge on SLET-driven corneal regeneration dependent on clinical studies and their limitations.[11–13] Here, we validated a mouse model of SLCET, i.e., a SLET-like approach adapted to the murine cornea, and evaluated its regenerative potential in a systemic and robust manner across time, with emphasis on the fate of the transplanted cells.

The induced alkali-injury reproduced the pathological features observed in LSCD patients, such as corneal conjunctivalization, vascularization, and loss of corneal integrity and thickness.[29,35] Additionally, it corroborated the interchange between corneal-specific (e.g., K12) and conjunctive-specific keratins (e.g. K19), the ablation of the expression of LSC markers (e.g., deltaNp63, ABCG2)[31,33,36] and the impairment of the proliferation and stemness potential, previously documented.[12–14,30,31,37,38]

The long-term efficacy of SLCET was inferred by extending the analysis to 40DPT, thus adapting the usual patient's follow-up of 6-12 months post-SLET[29,35,39] to the fast-aging of mice (26 times faster).[40] SLCET led to a striking and persistent prevention of corneal conjunctivalization and vascularization, prevented the corneal nuclei loss associated with injury progression, and was the only experimental group that increased the K12$^+$-cells. Similarly, co-transplantation of limbal epithelial and stromal cells promoted the expression of corneal-keratins and disfavored the corneal neovascularization and conjunctivalization.[13]

In agreement with the anti-inflammatory properties of AM,[6–8] both INJ-SLCET and INJ-AMT groups displayed an immunomodulatory effect, lowering the macrophage infiltration. Despite the AMT favoring the microenvironment for the expansion of the trauma-surviving LSC,[41,42] only SLCET promoted a persistent restoration of deltaNp63 and ABCG2 expression, consequently ameliorating the limbal-corneal stemness. Such increments in the expression of stemness and self-renewal regulation proteins are often interpreted as a replenishment of lost LSC niches.[13,21,37]

Expression of K19 and K14, both associated with human LSC,[16,30] was differentially expressed in the murine cornea. A minimum co-expression of ABCG2/K19 was observed, with K19$^+$-cells occurring at the superficial corneal layer, while the K14$^+$-cells were almost absent from the healthy cornea, increasing only after injury, as previously reported.[36,43] Importantly, INJ-SLCET reverted K14 expression to physiological levels, suggesting that the transient increase of this population constitutes an insult response and its long-term presence indicates abnormal healing, in mice. Finally, the increase of K12-, Nestin-, and Ki67$^+$-cells suggested a persistent replenishing effect of the corneal population and improvement of the corneal stemness and proliferative potentials after SLCET. Noteworthy, we made a pioneering evaluation of the functional impact of LSCD, using TOCs, an increasingly used technology for vision testing in rodents.[44,45] The reduction of K19 expression after SLCET was associated with an improvement in the visual discrimination, suggesting that the recovery of the corneal morphological properties may lead to the improvement of its refractive functions, essential for vision acuity.[46]

area (K12, red, delimited by dashed lines) was used to identify the keratinized epithelium (opposing arrowheads), and the corneal thickness was assessed. (C) Corneal conjunctivalization was assessed by the keratin-19$^+$-area (K19, green) in the corneal epithelium. (D) Detection of corneal deltaNp63-expressing cells (red, white arrows). (E) Graph expressing the number of nuclei at both timepoints. (F) Graph representing the number of different corneal populations. (G) Graph expressing the percentage of K12$^+$-cells in the corneal epithelium. (H) Graph expressing the corneal epithelial thickness. (I) Graph expressing the percentage of K19$^+$-area. (J) Graph expressing the number of deltaNp63$^+$ cells in the corneal epithelium. (K) Detection of the corneal ABCG2- (red, white arrows) and K19-expressing cells (green) in the peripheral cornea. ABCG2 and K19 were largely mutually exclusive. (L) Detection of K14- (green) and K12-expressing cells (red). Single K14$^+$-cells are indicated with arrowheads, while K14$^+$/K12$^+$-cells are identified with arrows. (M) Graph expressing the number of ABCG2$^+$ and ABCG2$^+$/K19$^+$-cells in the peripheral corneal epithelium. (N) Graph expressing the number of K14$^+$ and K14$^+$/K12$^+$-cells in the corneal epithelium. (O) Graph expressing the impact of the alkali-injury in a pairwise discrimination, as a percentage of correct trials. (P) Graph expressing the inverse correlation between conjunctivalization (K19 expression) and the visual function (% of correct trials). The peripheral corneal epithelium comprises the limbal cornea. Scale bar: 50 µm (A-C) or 25 µm (D, K, L). Data were plotted as mean ± SEM (One-way ANOVA with Tukey's post-hoc test; two-tailed Pearson correlation; $N = 3$). **P*-value <.05, ***P*-value <.01, ****P*-value <.001, *****P*-value <.0001.

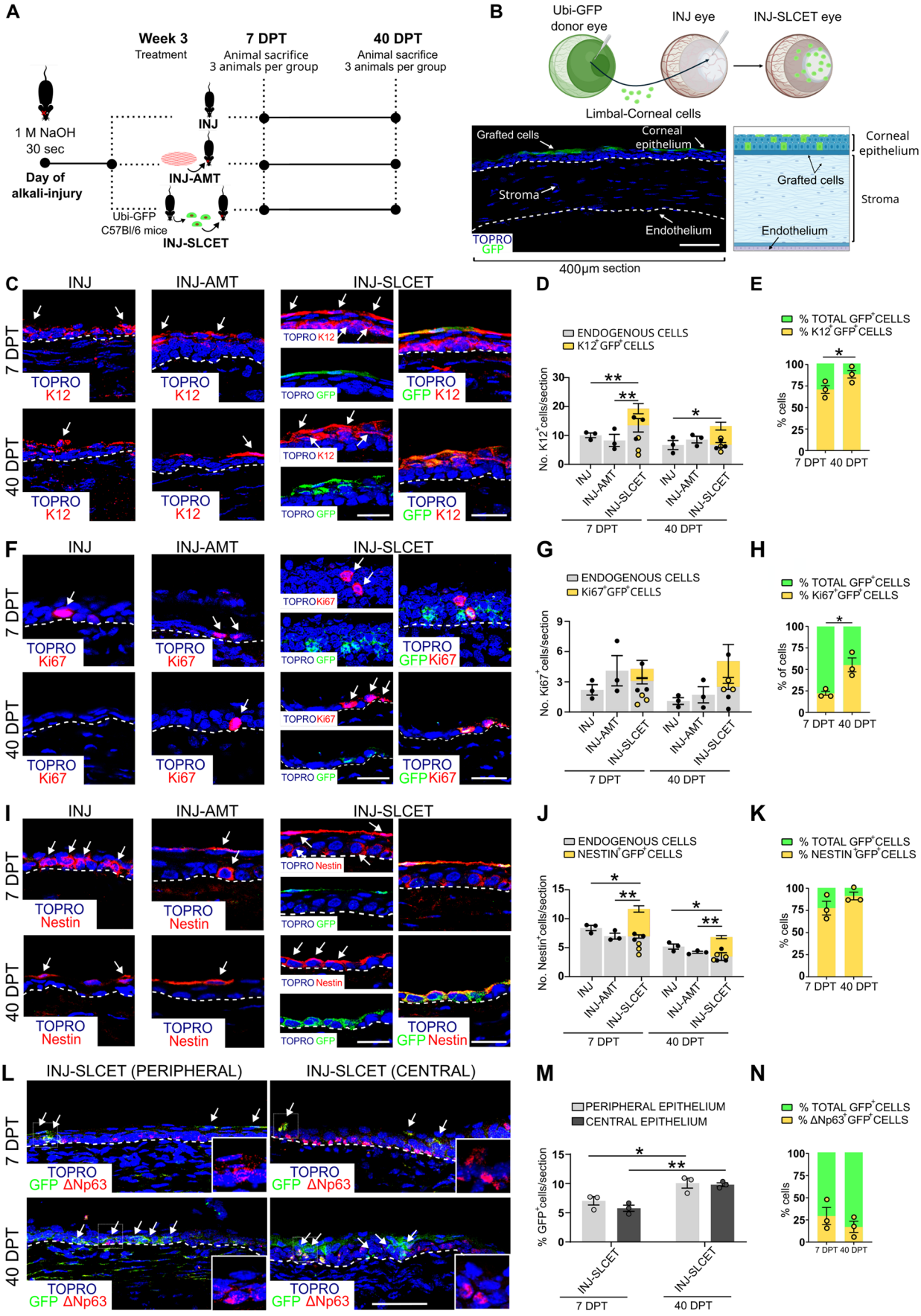

Figure 4. Simple limbal-corneal epithelial transplantation (SLCET) promoted stemness in the injured corneal epithelium and contributed to maintaining long-term proliferative and stemness features. (A) Diagram of the experimental plan. The alkali-burn was done on the right eye, and mice were divided into 3 experimental groups, 3 weeks after injury. One group was left untreated (injured non-treated group; INJ), another underwent amniotic membrane

The engrafted-cells were evenly distributed across the cornea. The majority were K12⁺- and Nestin⁺-cells, with few being deltaNp63⁺-cells, suggesting that part of the engrafted-cells were transient amplifying cells, i.e., cells committed to terminal differentiation with limited proliferative capacity.[43] Nevertheless, the maintenance of a persistent proliferative potential and retention of deltaNp63 expression among the engrafted-cells support a long-term regenerative potential of SLCET for the treatment of LSCD and strongly suggest that SLCET was decisive to enlarge the corneal regenerative population in the damaged niche, in the present model.

Study limitations

The post-injury expression of K12, deltaNp63, and ABCG2 indicates a partial LSCD that could allow some spontaneous healing.[47] Nevertheless, the regenerative effect of SLCET was superior to AMT, suggesting that the recovery of the INJ-SLCET group was not exclusively driven by the surviving resident limbal-corneal cells. Instead, our data suggested that the engrafted-cells played a crucial role in accelerating the corneal regeneration. This study used a murine model. Mice are small-sized animals, and their handling imposes methodological limitations.[24,48] Besides, humans and mice present interspecies differences on LSCs distribution: while human LSCs are restricted to the limbus, slow-cycling stem-like cells are distributed across the entire murine cornea.[2,3,25] Therefore, we replaced the limbal biopsy with the limbal-corneal debridement, to overcome the lack of an anatomically well-defined SC niche.[3] Although less precise, this approach enabled the implementation of an easy and affordable SLET-like model, offering a valuable platform to dissect SLET-driven regenerative mechanisms and identify modulators that enhance its efficacy. Additionally, the possibility to use different genetically-modified mice strains with clinical relevance represents another advantage of an SCLET murine model.[49]

Conclusion

We provided a novel and comprehensive characterization of the short- and long-term effects of SLCET, a SLET-based single-stage corneal transplantation, in an alkali-injury murine model. The results demonstrated a lasting reduction of the corneal opacification and vascularization, attenuation of the inflammatory response, and recovery of the physiological corneal phenotype. Our work highlighted the dynamic nature of corneal lesions and regeneration and the importance of the synergic involvement of endogenous and engrafted-cells for corneal regeneration. The described framework holds a high translation potential to expand our knowledge about the molecular pathways that regulate SLET-driven corneal regeneration and for the discovery of novel LSC modulators to develop new therapeutic strategies for the LSCD.

Acknowledgments

The authors acknowledge Alberto Poli and Sofia Massaro for helping with the immunostaining. The "Centro Interdipartimentale di Servizi per la Ricerca che utilizza Animali da Laboratorio"—C.I.R.S.A.L. and "Centro Piattaforme Tecnologiche"—CPT (University of Verona) are acknowledged for the services and support.

Author contributions

Marcia F.D. Costa, Nicola Piazza, and Erika Bonacci are considered co-first authors and Ilaria Decimo is considered the lead contact.

Márcia F.D. Costa (Data curation [equal], Formal analysis [equal], Investigation [equal], Visualization [equal], Writing—original draft [equal], Writing—review & editing [equal]), Nicola Piazza (Data curation [equal], Formal analysis [equal], Investigation [equal], Visualization [equal], Writing—original draft [equal], Writing—review & editing [equal]), Erika Bonacci (Data curation [equal], Investigation [equal], Writing—review & editing [equal]), Sissi Dolci (Conceptualization [supporting], Formal analysis [supporting], Investigation [equal], Writing—original draft [supporting], Writing—review & editing [supporting]), Francesca Ciarpella (Formal analysis [supporting], Visualization [equal], Writing—original draft [supporting], Writing—review & editing [supporting]), Marzia Di Chio (Formal analysis [supporting], Investigation [equal], Visualization [supporting], Writing—review & editing [supporting]), Stefania Zorzin (Investigation [supporting], Writing—review & editing [supporting]), Andrea Corsi (Investigation [supporting], Writing—review & editing [supporting]), Alessandro Piva

application (INJ-AMT), and the last group was submitted to SLCET procedure (INJ-SLCET) using cells transplanted from a Ubi-GFP C57Bl/6 mouse. Mice were then sacrificed at either 7- or 40-days post-treatment (DPT) for analysis. (B) Schematic representation of the SLCET procedure performed on INJ-SLCET mice. The eyes of Ubi-GFP C57Bl/6 mice were scraped to collect limbal-corneal cells and transplant them along with the AM into the injured receiver eye. The engrafted-cells were tracked by analyzing the GFP⁺-cells present in the cornea. (C) Confocal representative images of keratin-12⁺-cells (K12, red, white arrows). Red and green color splits for the INJ-SLCET group are presented. (D) Graph reporting the number of corneal K12⁺-cells. For the INJ-SLCET group, the yellow portion of the column represents the number of K12⁺/GFP⁺-cells, highlighting the engrafted-cell contribution to the increase in K12⁺-cells. (E) Graph representing the percentage of K12⁺/GFP⁺-cells over the total number of GFP⁺-cells. The green bar represents a visual aid of the percentage of total GFP⁺-cells (100%). (F) Representative confocal images of Ki67⁺-cells (red, white arrows). Red and green color splits for the INJ-SLCET group are presented. (G) Graph reporting the number of Ki67⁺-cells in the cornea. For the INJ-SLCET group, the yellow portion of the column represents the number of Ki67⁺/GFP⁺-cells counted, highlighting the engrafted-cell contribution to the increase in Ki67⁺-cells. (H) Graph representing the percentage of Ki67⁺/GFP⁺-cells over the total number of GFP⁺-cells. The green bar represents a visual aid of the percentage of total GFP⁺-cells (100%). (I) Representative confocal images of Nestin⁺-cells (red, white arrows). Red and green color splits for the INJ-SLCET group are presented. (J) Graph reporting the number of Nestin⁺-cells in the cornea, for the INJ-SLCET group, the yellow portion of the column represents the number of Nestin⁺/GFP⁺-cells counted, highlighting the engrafted-cell contribution to the increase in Nestin⁺-cells. (K) Graph representing the percentage of Ki67⁺/GFP⁺ cells over the total number of GFP⁺-cells. The green bar represents a visual aid of the percentage of total GFP⁺-cells (100%). (L) Representative confocal images of GFP⁺ (green, white arrows) and deltaNp63⁺-cells (red), in the peripheral and central cornea of the INJ-SLCET group. Digital magnifications of the red color splits from the deltaNp63⁺-cells are presented. (M) Graph reporting the number of GFP⁺-cells housed in the peripheral and central cornea. (N) Graph representing the percentage of deltaNp63⁺/GFP⁺-cells over the total number of GFP⁺-cells. The green bar represents a visual aid of the percentage of total GFP⁺-cells (100%). The peripheral corneal epithelium comprises the limbal cornea. Scale bar: 25 μm (C, F, I) or 50 μm (B, L). Data were plotted as mean ± SEM (One-way ANOVA with Tukey's post hoc test or two-tailed unpaired *t*-test when only two groups were analyzed; $N=3$). **P*-value <.05, ***P*-value <.01.

(Formal analysis [supporting], Investigation [supporting], Writing—review & editing [supporting]), Cristiano Chiamulera (Formal analysis [supporting], Writing—review & editing [supporting]), Zulkifal Malik (Formal analysis [supporting], Investigation [supporting], Writing—review & editing [supporting]), Riccardo Esposito (Formal analysis [supporting], Investigation [supporting], Writing—review & editing [supporting]), Francesco Bifari (Formal analysis [supporting], Writing—review & editing [supporting]), Stefano Ugel (Investigation [supporting], Writing—review & editing [supporting]), Adriano Fasolo (Investigation [supporting], Writing—review & editing [supporting]), Antonella Motta (Formal analysis [supporting], Writing—review & editing [supporting]), Stefano Ferrari (Formal analysis [supporting], Writing—review & editing [supporting]), Emilio Pedrotti (Conceptualization [equal], Funding acquisition [equal], Investigation [supporting], Writing—review & editing [supporting]), and Ilaria Decimo (Conceptualization [equal], Formal analysis [supporting], Funding acquisition [lead], Supervision [Lead], Visualization [supporting], Writing—original draft [supporting], Writing—review & editing [supporting])

Supplementary material

Supplementary material is available at *Stem Cells Translational Medicine* online.

Funding

This work was funded by European Union—Next Generation EU, Mission 4 Component 1 CUP: E53D23007260006 as part of the PRIN program of Italian Ministry of University and Research (MUR; identification code 2022MBA887), the National Recovery and Resilience Plan (NRRP), project MNESYS (PE0000006) – A Multiscale integrated approach to the study of the nervous system in health and disease (DN. 1553 11.10.2022), by the European Union project FETPROACT-2018-2020 HERMES (grant number 824164), the National Recovery and Resilience Plan (NRRP), Mission 4 Component 2 Investment 1.4—Call for tender No. 3138 of 16 December 2021, rectified by Decree n.3175 of 18 December 2021 of Italian Ministry of University and Research funded by the European Union—NextGenerationEU, Project code CN_00000033, Concession Decree No. 1034 of 17 June 2022 adopted by the Italian Ministry of University and Research, CUP B33C22000660001, Project title "National Biodiversity Future Center—NBFC" and PRIN2022 (grant 2022LB4X3N). Nicola Piazza was supported by a PhD fellowship funded by the National Recovery and Resilience Plan (NRRP) by the D.M. 352/2022.

Conflicts of interest

The authors declare no potential conflicts of interest.

Data availability

The authors confirm that all data supporting the findings described in this paper are fully available without restriction within the paper and its online supplementary data. Any additional information required to reanalyze the reported data can be obtained from the lead contact upon request.

Ethics approval and consent to participate

The study titled "Establishing of pharmacological modulators for limbal epithelial stem cells (LESC) to improve the efficacy of simple limbal epithelial transplantation (SLET) in the treatment of Limbal Stem Cell Deficiency (LSCD)" was approved by the National Institute of Health (protocol no. 1013/2024-PR) on October 11, 2024. The animal housing and experimental procedures were approved by the National Institute of Health (I.S.S.; Istituto Superiore di Sanità), and by the Animal Ethics Committee (C.I.R.S.A.L.; Centro Interdipartimentale di Servizio alla Ricerca Sperimentale) of the University of Verona (Italy) (approval no. 9/2022-UT) on July 7, 2022.

Consent for publication

Written informed consent for publication was obtained from all patients included in the study.

References

1. Knupp C, Pinali C, Lewis PN, et al. The architecture of the cornea and structural basis of its transparency. *Adv Protein Chem Struct Biol*. 2009;78:25-49. https://doi.org/10.1016/S1876-1623(08)78002-7
2. Dua HS, Shanmuganathan VA, Powell-Richards AO, Tighe PJ, Joseph A. Limbal epithelial crypts: a novel anatomical structure and a putative limbal stem cell niche. *Br J Ophthalmol*. 2005;89:529-532. https://doi.org/10.1136/bjo.2004.049742
3. Li J, Xiao Y, Coursey TG, et al. Identification for differential localization of putative corneal epithelial stem cells in mouse and human. *Sci Rep*. 2017;7:5169. https://doi.org/10.1038/s41598-017-04569-w
4. Kao WW. Keratin expression by corneal and limbal stem cells during development. *Exp Eye Res*. 2020;200:108206. https://doi.org/10.1016/j.exer.2020.108206
5. Deng SX, Borderie V, Chan CC, et al.; The International Limbal Stem Cell Deficiency Working Group. Global consensus on definition, classification, diagnosis, and staging of limbal stem cell deficiency. *Cornea*. 2019;38:364-375. https://doi.org/10.1097/ICO.0000000000001820
6. Sanders FWB, Huang J, Alió Del Barrio JL, Hamada S, McAlinden C. Amniotic membrane transplantation: structural and biological properties, tissue preparation, application and clinical indications. *Eye (Lond)*. 2024;38:668-679. https://doi.org/10.1038/s41433-023-02777-5
7. Meller D, Pires RT, Mack RJ, et al. Amniotic membrane transplantation for acute chemical or thermal burns. *Ophthalmology*. 2000;107:980-989; discussion 990. https://doi.org/10.1016/S0161-6420(00)00024-5
8. Gomes JA, dos Santos MS, Cunha MC, Mascaro VL, Barros JN, de Sousa LB. Amniotic membrane transplantation for partial and total limbal stem cell deficiency secondary to chemical burn. *Ophthalmology*. 2003;110:466-473. https://doi.org/10.1016/S0161-6420(02)01888-2
9. Sangwan VS, Basu S, MacNeil S, Balasubramanian D. Simple limbal epithelial transplantation (SLET): a novel surgical technique for the treatment of unilateral limbal stem cell deficiency. *Br J Ophthalmol*. 2012;96:931-934. https://doi.org/10.1136/bjophthalmol-2011-301164
10. Borderie VM, Ghoubay D, Georgeon C, et al. Long-term results of cultured limbal stem cell versus limbal tissue transplantation in stage III limbal deficiency. *Stem Cells Transl Med*. 2019;8:1230-1241. https://doi.org/10.1002/sctm.19-0021
11. Thokala P, Singh A, Singh VK, et al. Economic, clinical and social impact of simple limbal epithelial transplantation for limbal stem cell deficiency. *Br J Ophthalmol*. 2022;106:923-928. https://doi.org/10.1136/bjophthalmol-2020-318642

12. Homma R, Yoshikawa H, Takeno M, et al. Induction of epithelial progenitors in vitro from mouse embryonic stem cells and application for reconstruction of damaged cornea in mice. *Invest Ophthalmol Vis Sci*. 2004;45:4320-4326. https://doi.org/10.1167/iovs.04-0044
13. Zhu L, Zhang W, Zhu J, et al. Cotransplantation of limbal epithelial and stromal cells for ocular surface reconstruction. *Ophthalmol Sci*. 2022;2:100148. https://doi.org/10.1016/j.xops.2022.100148
14. Lin KJ, Loi MX, Lien GS, et al. Topical administration of orbital fat-derived stem cells promotes corneal tissue regeneration. *Stem Cell Res Ther*. 2013;4:72-87. https://doi.org/10.1186/scrt223
15. Le Q, Xu J, Deng SX. The diagnosis of limbal stem cell deficiency. *Ocul Surf*. 2018;16:58-69. https://doi.org/10.3389/fmed.2022.836009
16. Schlötzer-Schrehardt U, Kruse FE. Identification and characterization of limbal stem cells. *Exp Eye Res*. 2005;81:247-264. https://doi.org/10.1016/j.exer.2005.02.016
17. Yoshida S, Shimmura S, Kawakita T, et al. Cytokeratin 15 can be used to identify the limbal phenotype in normal and diseased ocular surfaces. *Invest Ophthalmol Vis Sci*. 2006;47:4780-4786. https://doi.org/10.1167/iovs.06-0574
18. Kato N., Fukagawa K., Dogru M., Fujishima H., Tsubota K. Mechanisms of giant papillary formation in vernal keratoconjunctivitis. *Cornea*. 2006; 25(10 Suppl 1): S47-52.
19. Lin T, Zhang X, Lu Y, Gong L. TGFBIp mediates lymphatic sprouting in corneal lymphangiogenesis. *J Cell Mol Med*. 2019;23:7602-7616. https://doi.org/10.1111/jcmm.14633
20. Figueira EC, Di Girolamo N, Coroneo MT, Wakefield D. The phenotype of limbal epithelial stem cells. *Invest Ophthalmol Vis Sci*. 2007;48:144-156. https://doi.org/10.1167/iovs.06-0346
21. Li Y, Giovannini S, Wang T, et al.; TOR Centre. p63: a crucial player in epithelial stemness regulation. *Oncogene*. 2023;42:3371-3384. https://doi.org/10.1038/s41388-023-02859-4
22. Gonzalez G, Sasamoto Y, Ksander BR, Frank MH, Frank NY. Limbal stem cells: identity, developmental origin, and therapeutic potential. *Wiley Interdiscip Rev Dev Biol*. 2018;7:1–15. https://doi.org/10.1002/wdev.303
23. Pauklin M, Thomasen H, Pester A, Steuhl KP, Meller D. Expression of pluripotency and multipotency factors in human ocular surface tissues. *Curr Eye Res*. 2011;36:1086-1097. https://doi.org/10.3109/02713683.2011.608238
24. Nureen L, Biazik J, Carnell M, Di Girolamo N. A detailed survey of the murine limbus, its stem cell distribution, and its boundaries with the cornea and conjunctiva. *Stem Cells Transl Med*. 2024;13:1015-1027. https://doi.org/10.1093/stcltm/szae055
25. Majo F, Rochat A, Nicolas M, Jaoudé GA, Barrandon Y. Oligopotent stem cells are distributed throughout the mammalian ocular surface. *Nature*. 2008;456:250-254. https://doi.org/10.1038/nature07406
26. Efron N, Hollingsworth JG. New perspectives on keratoconus as revealed by corneal confocal microscopy. *Clin Exp Optom*. 2008;91:34-55. https://doi.org/10.1111/j.1444-0938.2007.00195.x
27. Kate A, Mudgil T, Basu S. Longitudinal changes in corneal epithelial thickness and reflectivity following simple limbal epithelial transplantation: an optical coherence tomography-based study. *Curr Eye Res*. 2022;47:336-342. https://doi.org/10.1080/02713683.2021.1988985
28. Ebenezar OO, Roney A, Goswami DG, et al. Ocular injury progression and cornea histopathology from chloropicrin vapor exposure: relevant clinical biomarkers in mice. *Exp Eye Res*. 2023; 230:109440. https://doi.org/10.1016/j.exer.2023.109440
29. Pedrotti E, Chierego C, Cozzini T, et al. In vivo confocal microscopy of the corneal-conjunctival transition in the evaluation of epithelial renewal after SLET. *J Clin Med*. 2020;9:3574. https://doi.org/10.3390/jcm9113574
30. Ramirez-Miranda A, Nakatsu MN, Zarei-Ghanavati S, Nguyen CV, Deng SX. Keratin 13 is a more specific marker of conjunctival epithelium than keratin 19. *Mol Vis*. 2011;17:1652-1661. http://www.molvis.org/molvis/v17/a183/
31. Kadar T, Horwitz V, Cohen M, et al. Limbal stem cell deficiency (LSCD) in rats and mice following whole body exposure to sulfur mustard (SM) vapor. *Exp Eye Res*. 2022;223:109195. https://doi.org/10.1016/j.exer.2022.109195
32. Swarup A, Ta CN, Wu AY. Molecular mechanisms and treatments for ocular symblephara. *Surv Ophthalmol*. 2022;67:19-30. https://doi.org/10.1016/j.survophthal.2021.04.008
33. Lin Z, He H, Zhou T, et al. A mouse model of limbal stem cell deficiency induced by topical medication with the preservative benzalkonium chloride. *Invest Ophthalmol Vis Sci*. 2013;54:6314-6325. https://doi.org/10.1167/iovs.12-10725
34. Kameishi S, Sugiyama H, Yamato M, et al. Remodeling of epithelial cells and basement membranes in a corneal deficiency model with long-term follow-up. *Lab Invest*. 2015;95:168-179. https://doi.org/10.1038/labinvest.2014.146
35. Mittal V, Jain R, Mittal R. Ocular surface epithelialization pattern after simple limbal epithelial transplantation: an in vivo observational study. *Cornea*. 2015;34:1227-1232. https://doi.org/10.1097/ICO.0000000000000573
36. Park M, Richardson A, Pandzic E, et al. Visualizing the contribution of keratin-14. *Stem Cell Reports*. 2019;12:14-28. https://doi.org/10.1016/j.stemcr.2018.11.014
37. Lee H, Lee JH, Hong S, et al. Transplantation of human corneal limbal epithelial cell sheet harvested on synthesized carboxymethyl cellulose and dopamine in a limbal stem cell deficiency. *J Tissue Eng Regen Med*. 2021;15:139-149. https://doi.org/10.1002/term.3159
38. Chan EH, Chen L, Rao JY, Yu F, Deng SX. Limbal basal cell density decreases in limbal stem cell deficiency. *Am J Ophthalmol*. 2015;160:678-684.e4. https://doi.org/10.1016/j.ajo.2015.06.026
39. Wang Y, Hu X, Yang K, et al. Clinical outcomes of modified simple limbal epithelial transplantation for limbal stem cell deficiency in Chinese population: a retrospective case series. *Stem Cell Res Ther*. 2021;12:259-269. https://doi.org/10.1186/s13287-021-02345-2
40. Agoston DV. How to translate time? The temporal aspect of human and rodent biology. *Front Neurol*. 2017;8:92. https://doi.org/10.3389/fneur.2017.00092
41. Rendal-Vázquez ME, San-Luis-Verdes A, Yebra-Pimentel-Vilar MT, et al. Culture of limbal stem cells on human amniotic membrane. *Cell Tissue Bank*. 2012;13:513-519. https://doi.org/10.1007/s10561-012-9300-x
42. Meller D, Pires RT, Tseng SC. Ex vivo preservation and expansion of human limbal epithelial stem cells on amniotic membrane cultures. *Br J Ophthalmol*. 2002;86:463-471. https://doi.org/10.1136/bjo.86.4.463
43. Tanifuji-Terai N, Terai K, Hayashi Y, Chikama T, Kao WW. Expression of keratin 12 and maturation of corneal epithelium during development and postnatal growth. *Invest Ophthalmol Vis Sci*. 2006;47:545-551. https://doi.org/10.1167/iovs.05-1182
44. Crijns E, Op de Beeck H. The visual acuity of rats in touchscreen setups. *Vision (Basel)*. 2019;4:4. https://doi.org/10.3390/vision4010004
45. Buscher N, van Dorsselaer P, Steckler T, Talpos JC. Evaluating aged mice in three touchscreen tests that differ in visual demands: Impaired cognitive function and impaired visual abilities. *Behav Brain Res*. 2017;333:142-149. https://doi.org/10.1016/j.bbr.2017.06.053
46. Riau AK, Look Z, Yam GHF, et al. Impact of keratocyte differentiation on corneal opacity resolution and visual function recovery in male rats. *Nat Commun*. 2024;15:4959. https://doi.org/10.1038/s41467-024-49008-3
47. Shanbhag SS, Chanda S, Donthineni PR, Basu S. Surgical management of unilateral partial limbal stem cell deficiency: conjunctival autografts versus simple limbal epithelial transplantation. *Clin Ophthalmol*. 2021;15:4389-4397. https://doi.org/10.2147/OPTH.S338894
48. Kethiri AR, Raju E, Bokara KK, et al. Inflammation, vascularization and goblet cell differences in LSCD: Validating animal models of corneal alkali burns. *Exp Eye Res*. 2019;185:107665. https://doi.org/10.1016/j.exer.2019.05.005
49. Loiseau A, Raîche-Marcoux G, Maranda C, Bertrand N, Boisselier E. Animal models in eye research: focus on corneal pathologies. *Int J Mol Sci*. 2023;24:1–42. https://doi.org/10.3390/ijms242316661.